

Electrical Characteristics of a Linear, Nonequilibrium, MHD Generator

BERT ZAUDERER* AND ERIC TATE†
General Electric Company, King of Prussia, Pa.

The purpose of this experimental study was to determine the electrical performance of a linear, segmented-electrode, MHD generator. Various noble gases were shock-heated to plasma conditions which allowed MHD generator operation with Hall parameters $\omega_e \tau_e$ ranging from 1 to 20 and ratios of electron to static gas temperatures of 1 to 2.5. For $T_e/T_g > 1$, the discharge structure in the generator was nonuniform. The major results were: 1) By comparing the experiments with an MHD generator theory that included the effect of nonuniform extrathermal ionization, it was found that the Faraday generator operated in the normal mode in which the current vector is approximately perpendicular to the axial flow direction, at all values of $\omega_e \tau_e$. The electrical performance of the generator at high $\omega_e \tau_e$ was much better than that predicted for the shorted mode of operation in which the current vector is inclined in the axial Hall direction. 2) It was found that it was possible to obtain good agreement between the experiments and a simple uniform plasma, segmented-electrode theory that included the Lorentz force effects, the electrode voltage losses, and the increased dissipation due to the plasma nonuniformities in the analyses. 3) Because of the relatively coarse electrode segmentation, it could not be established conclusively whether the effect of the electrothermal instabilities or the effect of finite electrode segmentation limited the maximum attainable Hall field.

Nomenclature

a	= speed of sound, m/sec
B	= magnetic field, webers/m ²
D	= channel width, cm
d	= width of current path in z direction, cm
E	= electric field, v/m
I	= current, amp
J, j	= current density, amp/cm ²
k	= Boltzmann's constant, 1.38×10^{-16} erg deg ⁻¹
L	= MHD generator length, m
l	= width of current path in x direction, cm
M	= (without subscript) atom mass of more abundant gas species, amu; (with subscript) Mach number
m	= electron mass, amu
n	= electron density, cm ⁻³
P	= pressure
S	= mean square deviation of electron density fluctuation
T	= temperature, °K
U	= velocity, m/sec
V	= voltage, v
X	= axial distance used in computing interaction parameter, m
x	= distance in axial, \mathbf{U} direction
y	= distance in transverse, $\mathbf{U} \times \mathbf{B}$ direction
z	= distance in transverse, \mathbf{B} field direction
δ_{eff}	= effective elastic collision loss factor, defined in Ref. 5
δ_T, δ_U	= thermal and velocity boundary-layer thickness, respectively, cm
ρ	= $\frac{1}{2}$ electrode segmentation ratio = $\frac{1}{2}$ axial electrode pitch/ D
θ	= $\tan^{-1}(j_x/j_y)$

τ_e	= electron-heavy-particle collisional mean free time
σ	= electrical conductivity
σ_{eff}	= ratio of current to field component in its direction
ω_e	= electron cyclotron frequency
$(\omega_e \tau_e)_{eff}$	= tangent of angle between \mathbf{J} and \mathbf{E}

Superscript

()*	= measurement in frame of reference moving with plasma
------	--

Subscripts

B	= effective electrical conductivity at given magnetic field strength
e	= electron
g	= conditions at gas temperature
i	= ambient conditions in front of incident shock
s	= combined sheath and boundary-layer voltage loss at electrodes
x, y, z	= Cartesian coordinates
0	= scalar conductivity

I. Introduction

It has been demonstrated¹ that the induced electric fields in a linear MHD generator can produce a nonequilibrium plasma in which the electron temperature is significantly greater than the gas stagnation temperature. Optical observations² of the plasma in the generator showed that the plasma luminosity was nonuniform in both the axial (gas velocity) and transverse (magnetic field) directions. Specifically, the luminosity was concentrated in streamers which were transverse to the gas flow and which were convected at the local gas velocity. The purpose of the present investigation was to determine the voltage-current characteristics of a linear MHD generator in the presence of a nonequilibrium plasma having the aforementioned nonuniformities.

Various theories³⁻⁶ have been used to describe the electrical characteristics of the linear nonequilibrium generator. It was previously found^{7,8} that, by considering the measured electrode voltage loss as an equivalent external impedance, the experimental Faraday-generator load lines at $\omega_e \tau_e \approx 1$

Received May 1, 1968; revision received May 29, 1968. Parts of the experimental results in this paper were presented at the Eighth Symposium on the Engineering Aspects of MHD, held at Stanford University in 1967. The authors wish to thank G. S. Argyropoulos of the STD Research Corporation for many useful discussions and for performing the numerical analyses in which the theory of Argyropoulos, Demetriades, and Kendig⁵ was applied to the experimental conditions. This work was supported in part by the Office of Naval Research.

* Group Leader, Pulsed MHD Power Generation. Member AIAA.

† Physicist, MHD.

and $T_e/T_g \approx 1$ were in good agreement with the finitely segmented electrode theory.³ However, at high-current levels the Hall voltages were up to a factor of 2 below the values predicted by this theory. Kerrebrock⁴ suggested that concentrated, extrathermal ionization at the finite-electrode segments would lead to the formation of an axial high-conductivity layer on the electrode walls. These layers would reduce the electrical performance of the generator at $\omega_e \tau_e \gg 1$ and $(T_e/T_g) > 1$. In an extension of the two preceding theories, Argyropoulos et al.⁵ and others^{9,10} have numerically solved the electron conservation equations and Ohm's law for a single finite-electrode pair in a linear MHD generator. Argyropoulos⁵ included the effect of finite reaction rates and electron thermal diffusion in the analysis. Nonuniformities in the magnetic field direction, which were observed in the MHD channel,² were neglected. Plasma nonuniformities and turbulence at high $\omega_e \tau_e$ are also predicted by the electrothermal instability theories.^{11,12} Assuming that the turbulent plasma has a specified structure, the average electrical impedance of the plasma has been derived.^{6,13,14} However, the effect of finite-electrode segmentation was neglected in the instability analysis.^{6,12-14} It should be noted that the theories of Kerrebrock,⁴ Argyropoulos,⁵ and Mitchner¹⁰ also predict the existence of instabilities at $\omega_e \tau_e > 1$. The experimental results will be compared with various predictions of the preceding theories.

The experiments were performed in the previously described^{1,2} 4.85-cm² shock tube in which a 4.85-cm² × 28-cm-long MHD generator was located at its downstream end. Xenon, xenon + 0.1% hydrogen, argon, and a 98% neon + 2% xenon mixture were utilized as the test gases. These gases were selected to obtain generator operation with $\omega_e \tau_e$ values in the plasma ranging from 1 to 20 and T_e/T_g ratios ranging from 1 to 2.5. The shock tube produced a hot gas slug that was about 50 cm long. The considerations entering in the selection of test gases will be given in Sec. IV. All the experiments were performed with the generator connected in the Faraday mode of operation.

II. MHD Channel and Experimental Techniques

There were 30 electrode pairs in the MHD channel.^{1,2} The axial electrode pitch of the flush mounted (4.70 cm long × 0.33 cm wide) copper electrodes was 0.96 cm, and the electrode segmentation ratio was 0.2. The electrode area used to compute the current density was (4.70 × 0.96) cm². The experiments were performed at magnetic field strengths of 0.735, 1.44, and 2.2 webers/m².

To obtain readily interpretable Hall potential data, the Hall voltage measurements were taken downstream of the ionization and current relaxation region in the channel where I_y was approximately constant. In the pure xenon, argon, and 98% neon + 2% xenon experiments, the $\mathbf{U} \times \mathbf{B}$ fields were too small to obtain the desired range of transverse current levels. Two methods were used to obtain a region of constant current level in the MHD channel. In some of the argon and all of the 98% neon + 2% xenon experiments, preionization was applied upstream of the MHD generator to increase the ionization rate and, hence, the maximum attainable current in the generator. In the other argon and in the pure xenon experiments, an electrically isolated capacitor and a limiting resistor were connected to each electrode pair. Both the capacitor voltage, which was applied to the electrodes in the $\mathbf{U} \times \mathbf{B}$ direction, and the electrode current were approximately constant during the 500- μ sec. test time. With this external voltage circuit, it was necessary to maintain the axial variation of I_y to less than 10% in the region where E_x was measured. For larger axial variations of I_y , large transverse variations in the Hall field were observed. For constant I_y along the channel, the

average Hall field was independent of the method used to obtain the desired current levels.

The following measurements were made: I_y was measured at up to 8 equally spaced electrode locations in the channel. The Hall voltages were measured, at the anode and cathode walls, over distances of ten or more axial electrode segmentation widths. Three sets of metal probes, protruding $\frac{1}{4}$ in. into the freestream, were located on one of the insulator walls of the channel at the 5th, 15th, and 25th electrode pairs. Each set consisted of three collinear probes that were transverse to the gas flow direction. The outer two probes were $\frac{7}{16}$ in. from the anode and cathode walls, respectively, and the middle probe was on the centerline of the insulator wall. The probes were used to measure the Faraday and Hall voltages. To prevent an accumulation of errors resulting from subtracting large numbers, all the voltages were measured differentially. Voltage measurements were obtained by connecting two Tektronix type P6006 voltage probes having a 10⁷-ohm input resistance and a 15 × 10⁻¹²-farad distributed capacity to two electrodes or two probes in the channel. The P6006 probe outputs were connected to a Tektronix type D differential, oscilloscope preamplifier. The continuum radiation of the plasma at 4800 Å was measured at the 7th and 20th electrode pair locations. The method of calibrating the radiation data is given in Ref. 1. Finally, the initial gas conditions at the generator entrance were computed from the measured shock velocity and the initial gas pressure, and the results will be given in Sec. IV.1.

III. Segmented-Electrode Generator Theory

The experiments will be compared to the finitely-segmented-electrode, MHD generator theory³ under the assumption that the plasma is in a uniform nonequilibrium state. Although the plasma is nonuniform,² this theory serves as a useful first approximation of the generator performance. The transverse current density j_y and the Hall field E_x are given by³:

$$j_y = \{ \sigma_0 / [1 + 2\rho(\omega_e \tau_e - 0.4)] \} [U_x B_z - E_y - E_s] = \sigma_{\text{eff}} [U_x B_z - E_y - E_s] \quad (1)$$

$$E_x = \{ \omega_e \tau_e / [1 + 2\rho(\omega_e \tau_e - 0.4)] \} [U_x B_z - E_y - E_s] = (\omega_e \tau_e)_{\text{eff}} [U_x B_z - E_y - E_s] \quad (2)$$

where E_y is the field due to the external load and E_s is the field due to the voltage loss in the electrode sheath and the cold aerodynamic boundary layer. σ_0 and τ_e are obtained by combining the steady-state electron energy equation,

$$j_y^2 / \sigma = 3(n_e / \tau_e) \cdot (m_e / M) \delta_{\text{eff}} k(T_e - T_g) \quad (3)$$

with the Saha equation. The resultant equation, which is given elsewhere,¹ enables one to compute T_e for a given j_y . From T_e all the other plasma properties are obtained.¹ Equations (1-3) are valid only if $j_x \ll j_y$ in the plasma. This condition is satisfied if the electrode segmentation ratio is much less than one (as is the case in the present experiments) and if no transverse nonuniformities exist in the plasma which can short the Hall field.⁴ Optical observations² of the discharge showed that the second condition appeared to be satisfied downstream of the entrance region of the generator. For a uniform plasma, σ in Eq. (3) should be replaced by σ_0 . Since the plasma is nonuniform,² one expects that for a given electrode current the dissipation and hence T_e in the plasma would exceed the value predicted with σ_0 . It was found¹ that replacing σ by σ_{eff} in Eq. (3) resulted in fairly good agreement with the electron density deduced from the measured continuum radiation in the generator. Since σ_{eff} is a function of the magnetic field B , the value of σ used in the theoretical anal-

Table 1 Plasma properties of the various test gases

Gas	1 P_i , torr	2 $M_s = U_i/a_i$	3 U_g , m/sec	4 P_g , atm	5 T_g , °K	6 $M_g = U_g/a_g$	7 j_y , amp/cm ²	8 T_e/T_g	9 n_e , cm ⁻³	10 $\omega_e\tau_e$ at 2.2 weber/m ²	11 σ_0 , mhos/m	12 δ_{eff}
Xenon + 0.1% hydrogen	8.25	8.10	1070	0.89	6330	1.30	2-35	1.01- 1.12	2×10^{15} - 5×10^{15}	4.5-2.5	480-900	1
Xenon	7.67	7.60	1000	0.73	5670	1.29	2-30	1.02- 1.22	5×10^{14} - 4×10^{15}	6.0-3.0	250-800	1
Xenon	9.00	7.10	925	0.74	5000	1.28	2-18	1.14- 1.30	4×10^{14} - 2×10^{15}	6.0-3.0	200-550	1
Argon	10.30	6.70	1580	0.76	4460	1.27	2-8	1.48- 1.66	10^{14} - 7×10^{14}	15.0-9.0	160-440	1
98% neon + 2% xenon	7.20	5.80	1810	0.37	3380	1.25	2-10	1.77- 2.12	10^{14} - 7.4×10^{14}	20.0-10.0	150-500	0.5-1
98% neon + 2% xenon	8.0	5.26	1635	0.36	2830	1.23	2-10	2.12- 2.50	10^{14} - 8×10^{14}	20.0-10.0	150-550	0.5-1

ysis of the generator voltage-current characteristics will be identified in the figures by the symbols $\sigma_B = 0$, $\sigma_B = 0.755$ webers/m², $\sigma_B = 1.44$ webers/m², and $\sigma_B = 2.2$ webers/m². In addition, to utilize the previous theory, one must show that the electrode voltage loss occurs in a region that is much smaller than the electrode segmentation pitch of the channel, $2\rho D$. This enables one to treat E_s as an equivalent external load. This assumption will be verified in Sec. V.1 of this paper. If this condition were not satisfied, the boundary-layer solution must be coupled to the electron conservation equations and Ohm's law to obtain the local distribution of the field near the electrodes.

The theoretical analysis of Argyropoulos⁵ was used to obtain additional verification of the validity of the assumption, which is implicit in Eqs. (1-3), that $\mathbf{J} \perp \mathbf{B}$ and $\mathbf{J} \perp \mathbf{U}$. In applying this theory to the present experimental conditions, the boundary conditions were that the plasma and field properties are periodic in the flow direction [e.g., $T_e(x,y) = T_e(x + 2\rho,y)$ and $\mathbf{J}(x,y) = \mathbf{J}(x + 2\rho,y)$]. On the electrode wall the boundary conditions are the following: on the electrode $E_x = 0$, and on the insulator $j_y = 0$. The electrodes are perfect electron emitters. The total current through the electrode pair, I_y , was specified. Thermal and velocity boundary layers were neglected. In the solution, a "constant-property" case is obtained first. It gives the uniform plasma properties and the local current and field distribution in one electrode pair segment. The local fields and currents are substituted into the electron conservation equations to obtain a first approximation of the nonuniform plasma properties. The solution is then iterated until it converges. The nonuniform plasma property solution will be called the "finite-rate" solution in subsequent discussions. In the core of the flow, the constant-property solution is identical with Eqs. (1-3) of this section with σ_0 substituted for σ in Eq. (3). The results of the computations will be discussed in Sec. V. The experiments will also be compared briefly with the ionization or electrothermal instability theories in Sec. V.

IV. Experimental Results and Discussion

1. Selection of Test Gases

It would have been desirable to cover the entire range of $\omega_e\tau_e$ and T_e/T_g values of interest in each test gas. However, this was not possible for the following reasons: 1) Based on optical observations² of the transverse streamer discharge pattern in the channel, it was concluded that, for I_y much less than 10 amp/electrode (i.e., $j_y \sim 2$ amp/cm²) and $T_e/T_g > 1$, the discharge did not fill a sufficient volume of the generator to enable one to assign an average state to the plasma in the generator. This lower limit on I_y resulted in a different lower limit on the average value of $\omega_e\tau_e$ and T_e/T_g in each of the test gases. 2) U_g was limited to less than 2000 m/sec. Hence, to exceed E_s , which ranged from 400 to 2000 v/m, B had to be greater than 0.5 webers/m². Ex-

ternal voltage sources were used to overcome E_s (see Sec. II). However, it was found that it was not possible to obtain useful Hall voltage data for $B_z < 0.5$ webers/m² because of the relatively large noise level of the experiments. 3) The upper limits of B_z and j_y were about 2 webers/m² and 30 amp/cm², respectively. Above these levels, the Lorentz force caused the formation of strong shock waves in the generator which resulted in large variations in I_y along the channel. Table 1 summarizes the properties of the various test gases. The first two columns show the initial conditions in front of the incident shock. Columns 3-6 show the computed local gas properties of the test gas entering the MHD channel. The range of j_y values utilized in the experiments is given in column 7. The remaining columns give the range of theoretical plasma properties corresponding to the j_y values in column 7. They were obtained by the method outlined in Sec. III and Ref. 1. The test gases in Table 1 are arranged in order of increasing $\omega_e\tau_e$ and T_e/T_g . Note that because of the coulomb cross sections $\omega_e\tau_e$ decreases with increasing j_y and T_e/T_g . Also, note that δ_{eff} is less than 1 in the 98% neon + 2% xenon gas mixture. This is caused by the coulomb effect and the disparity in particle mass between seed and parent gas.

The xenon experiments are an extension to higher $\omega_e\tau_e$ and T_e/T_g of previously reported studies in xenon.⁷ The presence of the 0.1% hydrogen in the xenon experiment at T_g of 6330°K increased the ionization rate behind the shock front. As a result, equilibrium plasma conditions were obtained within 20 cm behind the shock front. The electrical conductivity at equilibrium was a few hundred mhos/m. Optical observations of the plasma, more than 20 cm downstream of the shock front, showed that the discharge in the MHD generator was uniform. The voltage-current measurements in the xenon + 0.1% hydrogen experiments were taken in the uniform plasma region. This test-gas mixture was used as a basis of comparison with the other experiments. In all the other experiments as a result of the slow ionization rate behind the shock front, n_e at the end of the gas slug was a factor of 10 or more below the equilibrium value. Consequently, streamers were observed in the generator at all current levels.

2. Measurement of Vectors $\mathbf{U} \times \mathbf{B}$, E_y , and E_x

For the proper interpretation of the experiments, it is necessary to discuss the factors that affect the accuracy of the field measurements in the generator. To obtain the theoretical, open-circuit $\mathbf{U} \times \mathbf{B}$ field, the plasma electron density must be large enough to supply the current required by the voltage measuring circuit without appreciably perturbing the local potential in the plasma. It was previously reported⁸ that with the P6006 voltage probe and for $n_e > 10^{12}$ cm⁻³, over 90% of the theoretical $\mathbf{U} \times \mathbf{B}$ voltage was measured at the electrodes in the MHD channel. For $n_e \approx 10^{12}$ cm⁻³ and a voltage probe resistance of only 10^9 ohms, the experimental $\mathbf{U} \times \mathbf{B}$ was about 50% of the theoretical

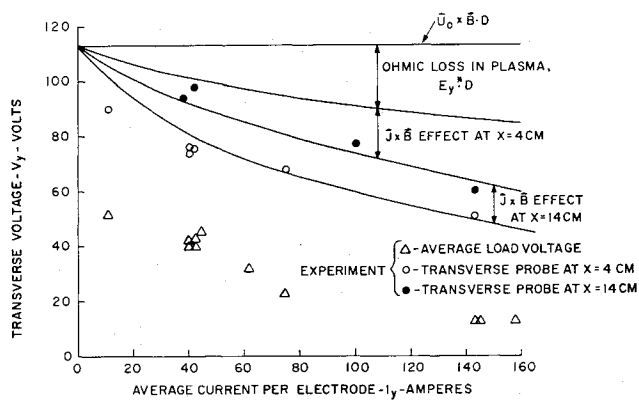


Fig. 1 Transverse voltage-current characteristics for the Faraday-generator experiments in the 99.9% xenon + 0.1% hydrogen mixture at $B_z = 2.2$ webers/m². The pertinent plasma properties are listed in Table 1. Note that the probe data are plotted as functions of I_y at the probe location. The variation of the probe data is $\pm 15\%$.

value. Similar low values of $\mathbf{U} \times \mathbf{B}$ were measured with the P6006 probe at $n_e \ll 10^{12}$ cm⁻³. In addition, in view of the short experimental test time, the voltage probe capacity had to be less than 10^{-11} farads to obtain sufficiently fast rise time of the voltage signal. The current collecting area of the metal probes on the insulator wall of the generator was 0.25 cm² compared to the 1.5 cm² electrode area. A free-stream n_e of more than 10^{13} cm⁻³ was required to obtain the theoretical $\mathbf{U} \times \mathbf{B}$ field with the metal probes.

The minimum average electron density in the loaded generator experiments was greater than 10^{14} cm⁻³ (Table 1). Thus in a uniform plasma, the metal probe measurements of the fields should be accurate at all values of I_y . This is not the case in the presence of streamers² since at low I_y the electron density outside the streamers can be much lower than the average n_e . In addition, the streamers cause electric field fluctuations having a frequency² of about 2×10^4 Hz. This reduces the a.c. impedance of the P6006 probe to 5×10^5 ohms compared to its 10^7 -ohms d.c. resistance. Since the streamers are parallel to $\mathbf{U} \times \mathbf{B}$, they primarily affect the accuracy of the transverse field measurement. Because of the small channel cross section, the maximum separation over which $(E_y + E_s)$ could be measured was 2.5 cm. This distance is comparable to the 1- to 3-cm axial separation of the streamers.² Hence, at any instance of time the two probes used to measure $(E_y + E_s)$ can be located in regions of the plasma having widely differing values of n_e . It is estimated then in the loaded generator experiments the maximum reduction in $(E_y + E_s)$ because of probe errors is about 30% (see Sec. IV.3). The minimum distance over which E_x was measured was four times the separation distance used in the E_y measurements. Hence, based on the $(E_y + E_s)$ error, it is estimated that the error in the probe measurements of E_x is less than 10%. As a result of the presence of large electrode losses, $(E_s + E_y)$ was always greater than 50% of $\mathbf{U} \times \mathbf{B}$. Hence, a relatively small error in $(E_y + E_s)$ causes an appreciable overestimate of E_y^* , where $E_y^* = \mathbf{U} \times \mathbf{B} - E_y - E_s$. Another factor affecting E_y^* is the gas flow deceleration caused by the Lorentz force. This deceleration was obtained from the measured propagation speed of the streamers.² The streamer velocity decreased with increasing $\mathbf{J} \times \mathbf{B} \cdot \mathbf{L} / \rho_0 U_0^2$. The velocity reduction was independent of the test gas used. It was shown² that the streamer velocity must be within 10% of the local gas velocity.

3. Faraday Generator: V_y - I_y Load Characteristics

In this section, the Faraday-generator load characteristics will be presented for the xenon + 0.1% hydrogen experiment

(Table 1, row 1) and for the 98% neon + 2% xenon experiment at $T_g = 2830^\circ\text{K}$ (Table 1, row 6). These experiments represent the two extremes of generator operation. In the former experiments, the plasma in the generator was uniform and $\omega_e \tau_e$ was small, whereas in the latter $\omega_e \tau_e$ was large and the streamer discharge pattern existed in the generator. The Faraday-generator load characteristics for the xenon + 0.1% H₂ experiments are shown in Fig. 1 for $B_z = 2.2$ webers/m². The load resistance at each of the 30 electrode pairs was varied from 5 to 0.1 ohms. For $I_y < 50$ amp/electrode, the plasma was approximately in equilibrium at the gas temperature. For $I_y > 140$ amps/electrode, the Lorentz force caused a considerable reduction in U_y , which resulted in a reduction of I_y at the downstream electrodes. Consequently, for $I_y > 140$ amp/electrode, only the average values of I_y in the upstream half of the channel are shown in Fig. 1. The theoretical ohmic voltage loss in the plasma, $E_y^* \cdot D$ in Fig. 1, was computed with Eqs. (1) and (3). $\sigma_{(B=2.2 \text{ webers/m}^2)}$ was substituted for σ in Eq. (3). If $\sigma_{(B=0)}$ had been used in Eq. (3), $E_y^* \cdot D$ would have been a few volts larger. To compare the probe data to the theory, the local gas velocity at the probe location was obtained from the graph of the streamer velocities as a function of $\mathbf{J} \times \mathbf{B} \cdot \mathbf{X} / \rho_0 U_0^2$, as outlined in Sec. IV.2. The magnitude of X was taken as the distance from the end of the current relaxation region at the channel entrance to the location of the transverse probe at which $(E_y + E_s)$ was measured. For the experiments shown in Fig. 1, I_y relaxed to its average value in the channel at the first electrode pair. Thus, the appropriate distances were $X = 4$ cm and $X = 14$ cm. The agreement between the two sets of probe measurements and the theory is good. Finally, by comparing the load voltages (triangular points) with the probe voltages (circular points in Fig. 1), one notes that the electrode voltage loss is about 40 v, and that is independent of I_y .

Figure 2 shows the Faraday-generator load characteristics for the 98% neon + 2% xenon experiment at $B_z = 2.2$ webers/m². The load resistance at each of the 30 electrode pairs was varied from 15 to 0.2 ohms. The method for computing $E_y^* \cdot D$ for these experiments was the same as that for Fig. 1, with $\sigma_{(B=2.2 \text{ webers/m}^2)}$ substituted in the electron energy equation. If σ_0 had been used, $E_y^* \cdot D$ would have been twice as large. However, as was noted in Sec. III, the local measurements of n_e in the generator were in considerably better agreement with the theoretical values obtained from Eq. (3) with $\sigma_{(B=2.2 \text{ webers/m}^2)}$. The transverse electric field, measured with the probes, increased in the downstream direction. This behavior is consistent with the effect of plasma nonuniformities on the probe circuit. As the plasma flows downstream, the discharge becomes more uniform, and the

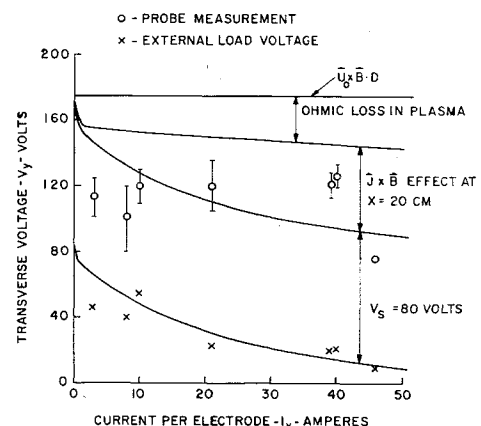


Fig. 2 Transverse voltage-current characteristics for the Faraday-generator experiments in the 98% neon + 2% xenon gas mixture at $T_g = 2830^\circ\text{K}$ and $B_z = 2.2$ webers/m². The pertinent plasma properties are given in Table 1.

accuracy of the probe circuit increases (see Sec. IV.2). Because of these effects, only the probe measurements obtained at the 15th and 25th electrode pair locations are shown in Fig. 2. The error flags on the probe measurements in Fig. 2 represent the range of the average values of the measured transverse electric field at these two probe locations. It will be noted that for $I_y < 45$ amp/electrode the average probe data increase slightly with I_y . Again, this is consistent with the observed discharge structure, since, with increasing I_y , more streamers form and the discharge becomes more uniform. Comparing the probe measurements with the theory at low I_y , one finds that the maximum reduction in $(E_y + E_s)$ due to probe errors is about 30%. Because of the uncertainties in the local transverse electric fields, only an approximate estimate of the Lorentz-force effect on U_a was made. In obtaining U_a at the probe location, a value of X of 15 cm was chosen for substitution into $J \times B \cdot X / \rho_a U_a^2$. 15 cm was the distance from the fifth electrode where I_y relaxes to its average value¹ to a position in the channel which is halfway between the aforementioned probe locations. As can be seen, the experimental probe data scatter around the theoretical curve that includes the effect of the Lorentz force and the ohmic voltage loss in the plasma. By subtracting a constant electrode voltage loss of 80 v from this curve, one obtains a new curve that is in excellent agreement with the measured voltage across the external load resistors. The agreement of the experiments with the uniform plasma, finite-electrode theory of Sec. III leads one to conclude that the generator operates in the normal mode (i.e., $J \perp B$ and U), regardless of the magnitude of $\omega_e \tau_e$, n_e , or T_e/T_p . This conclusion will be discussed in Sec. V.2.

4. Faraday Generator: Hall Voltage Measurements

To eliminate entrance effects on the Hall voltage measurements, a minimum of ten electrode pairs (i.e., a length of 2 channel diam) had to be externally loaded. In experiments in which only five electrode pairs had external loads, the measured Hall field was in some cases considerably greater than that obtained in a longer channel at the same I_y . The larger Hall field is due to the convective effect that displaces the discharge in the downstream direction. Since $\omega_e \tau_e$ decreases with increasing I_y , the Hall field in the inter-electrode space in the channel entrance region can be greater than the theoretical value at a given I_y . In the experiments discussed in this section, the number of electrode pairs (which were externally loaded) ranged from 13 to 30. Hall field measurements were taken at least 1 channel-diam downstream of the entrance region in a section of the generator where I_y was constant. Regardless of whether the current levels in the generator were obtained with external voltage sources or with load resistors (see Sec. II), a monotonic transverse asymmetry of the Hall field was observed. The minimum Hall field was

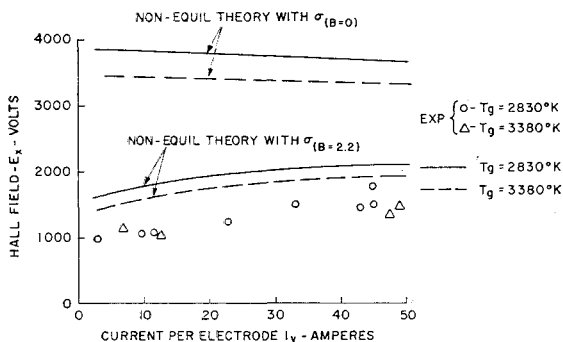


Fig. 3 Hall field as a function of the average current per electrode for the 98% neon + 2% xenon experiments (see Table 1) at $B_z = 2.2$ webers/m².

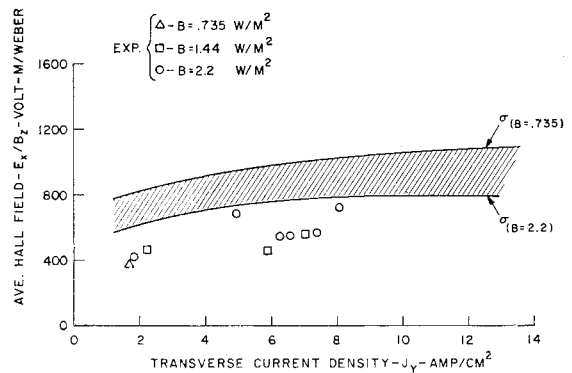


Fig. 4 Average reduced Hall field as a function of the average transverse current density for the argon experiments (see Table 1). The variation of the probe data is $\pm 20\%$.

at the anode wall and the maximum at the cathode wall. The Hall field variation obtained from the three probe measurements were always considerably less than that measured at the electrode walls. This discrepancy is attributed to the different magnitudes of the electrode voltage losses at the anodes and cathodes. The average of the three E_x measurements obtained with probes was always within 20% of E_x values measured with the central pair of probes. In the subsequent Hall data analysis, the average E_x obtained with the probes will be used. A possible cause of the E_x asymmetry will be given at the end of this section.

Figure 3 shows the Hall field as a function of the current per electrode for the 98% neon + 2% xenon experiments at $B_z = 2.2$ webers/m² and T_p of 2830° and 3380°K (see Table 1). The two sets of theoretical curves at T_p of 2830° and 3380°K were obtained from Eqs. (2) and (3) with σ_0 and $\sigma_{(B=2.2 \text{ webers/m}^2)}$ substituted in Eq. (3). It can be seen that the scatter in the data of the two experiments exceeds the effect of T_p in the two sets of theoretical curves. The experiment is within a factor of 2 below the two theoretical curves labeled $\sigma_{(B=2.2 \text{ webers/m}^2)}$. The deviation appears to be independent of I_y . It was previously reported¹ that the measured n_e in the generator was within a factor of 2 greater than the theoretical value obtained with $\sigma_{(B=2.2 \text{ webers/m}^2)}$. For fixed B_z and j_y , the product of $n_e E_x$ is a constant in a linear generator operating in the normal mode.¹ Thus E_x is below the $\sigma_{(B=2.2 \text{ webers/m}^2)}$ theoretical curve, because the corresponding experimental n_e is higher than the theoretical value.

Figure 4 shows the reduced Hall field as a function of j_y for the argon experiments. These experiments are similar to the 98% neon + 2% xenon experiments in that (T_e/T_p) and $\omega_e \tau_e$ are large (see Table 1). It can be seen that the argon Hall data show about the same factor of 2 deviation from the theory as show the 98% neon + 2% xenon data. As in the latter experiments, the measured electron densities of the argon generator were also within a factor of 2 greater than the theory. Thus, one can conclude that the presence of the seed in the noble gas has no measurable effect on the performance of this generator.

E_x/B_z as a function of j_y for the xenon experiments at T_p of 5670° and 5000°K (see Table 1) are shown in Figs. 5 and 6, respectively. For T_p of 5670°K and $j_y \leq 2$ amp/cm², the Hall field data scatter around the equilibrium theory at the gas temperature. For higher j_y values, the data scatter around the nonequilibrium theory. At $T_p = 5000$ °K, the crossover from equilibrium to nonequilibrium conditions occurs at $j \approx 0.5$ amp/cm², and all the data lie in the nonequilibrium region. It should be noted that in both sets of experiments n_e at the generator entrance was at least a factor of 10 below the equilibrium value (see Sec. IV.1). This can account for the relatively large scatter in the Hall

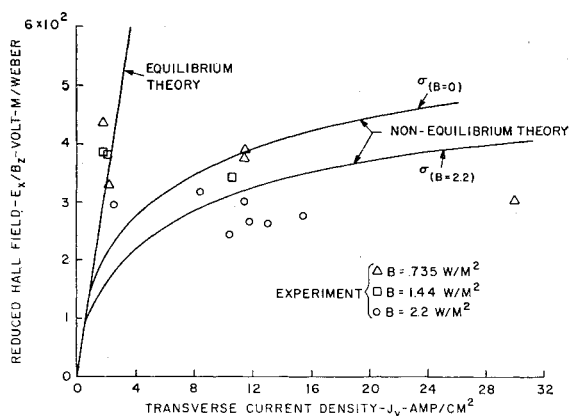


Fig. 5 Reduced Hall field vs transverse current density for the xenon experiments at $T_g = 5670^\circ\text{K}$ (see Table 1). The accuracy of the data is $\pm 20\%$.

data at $j \approx 2$ amp/cm² in Fig. 5, because $\omega_e \tau_e$ is above the equilibrium value inside the streamers and below the equilibrium value outside the streamers. The Hall data for the 6330°K experiments in xenon (see Table 1) are not shown. They were similar to the data in Fig. 5, except that the crossover from equilibrium to nonequilibrium conditions occurred at $j \approx 10$ amp/cm².

A number of aspects of the Hall data in Figs. 3-6 are of interest. One notes that, for fixed j_y in xenon (Figs. 5 and 6), the experimental E_x/B_z data decrease with increasing B_z . This behavior appears to be in agreement with the present theory in which σ_{eff} is used in the electron energy equation. However, this result is inconclusive since the experimental data of E_x/B_z in argon appear to be independent of B_z . It is possible to attribute the observed dependence of E_x/B_z on B_z in xenon to the effect of the Lorentz force. Similarly, the increasing deviation of the experimental Hall field below the theory, as j_y is increased (Figs. 5 and 6), can also be attributed to the Lorentz force. Figure 7 is a graph of the ratio of the experimental to the theoretical E_x as a function of $J \times B \cdot L/\rho_0 U_0^2$ for experiments shown in Figs. 3, 5, and 6. To simplify the comparison, the theoretical Hall field obtained with the $\sigma_{(B=0)}$ computation was used in obtaining the data for Fig. 7. One notes in Fig. 7 that $[(E_x)_{exp}/(E_x)_{theor}]$ in xenon decreases with increasing interaction parameter, regardless of the magnitude of B_z (i.e., $\omega_e \tau_e$). On the other hand, $[(E_x)_{exp}/(E_x)_{theor}]$ in the 98% neon + 2% xenon experiments increases with increasing interaction parameter. In xenon ($T_e/T_g \approx 1$). Hence, the plasma properties are very sensitive to changes in T_g . As $J \times B$ increases, T_g and n_e increase. Since for fixed j_y the

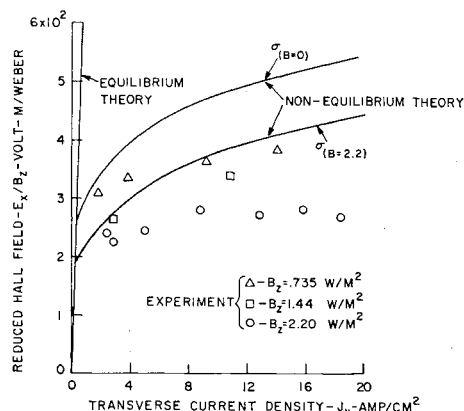


Fig. 6 Reduced Hall field vs transverse current density for the xenon experiments at $T_g = 5000^\circ\text{K}$ (see Table 1). The data accuracy is $\pm 20\%$.

product of $n_e E_x$ is a constant,¹ the effect of increasing $J \times B$ reduces E_x . This is in agreement with the trend shown by the experimental data in Figs. 5 and 6. On the other hand, in the 98% neon + 2% xenon experiments where (T_e/T_g) is relatively large, T_g has a very small effect on E_x (see Fig. 3). Hence, E_x should be independent of $J \times B$. The increase in E_x with increasing $J \times B$ is primarily due to the use of the $\sigma_{(B=0)}$ theoretical curve in preparing Fig. 7. If the $\sigma_{(B=2.2 \text{ webers/m}^2)}$ theoretical curve had been used, which is in much better agreement with the experiments (see Fig. 5), the 98% neon + 2% xenon data in Fig. 7 would have been more horizontal.

One final point of interest in connection with the Hall voltage is the observed asymmetry of E_x . The lower E_x at the anode walls indicates that local shorting of the Hall field is occurring, which can be caused by the presence of a high-conductivity gas layer on the wall. Such a layer has been observed⁸ on the anode wall at high Lorentz forces. The combined effect of the convective and Lorentz forces on the transverse streamers is in a direction that can drive the discharge into the anode wall. This effect is augmented by current constriction at the electrodes.² The degree of constriction required to obtain a $J \times B$ force induced deflection can be estimated as follows: Static pressure measurements on the MHD channel wall showed that for $J \times B \cdot L/\rho_0 U_0^2 > 0.05$ one obtains a measurable pressure rise. The current density can be approximated as I_y/l , where l is the width of the current path in the gas flow direction and d is its width in the B field direction. Substituting the xenon experimental conditions where a wall layer occurred⁸ [$B_z = 2.2$ webers/m², $I_y = 100$ amp, $\rho_0 U_0^2 \approx 2 \times 10^5$ N/m²] into the expression $J \times B \cdot L/\rho_0 U_0^2 = 0.05$, one obtains $d = 2.2$ mm. This width is consistent with those observed optically in the discharge. It should be noted that hot gas layers on the electrode wall can also be caused by nonuniform extrathermal ionization. This will be discussed in Sec. V.2.

V. Discussion of Generator Loss Mechanisms

1. Electrode Voltage Loss

In this section, it will be shown that most of the electrode voltage loss occurs in a region that is less than 1 mm from the electrode surface. Hence, it can be treated as an equivalent external voltage loss in the generator analysis. The measured V_s values, obtained from the probes in the channel, ranged from 20 v at $n_e > 10^{15}$ cm⁻³, $T_e/T_g \approx 1$, and $\omega_e \tau_e \approx 0$

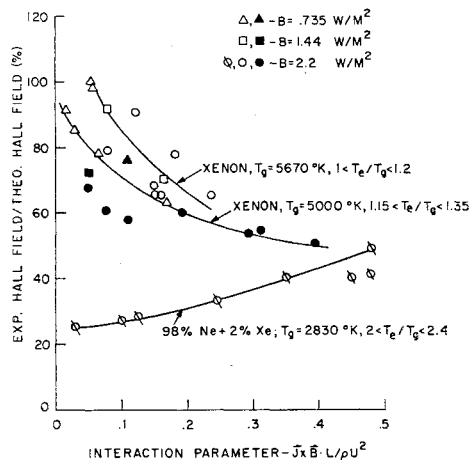


Fig. 7 Experimental Hall field divided by the theoretical Hall field as a function of the electromagnetic interaction parameter $J \times B \cdot L/\rho U^2$ for the xenon and one of the 98% neon + 2% xenon experiments. Note that the scalar conductivity was used in Eq. (3) in deriving the theoretical Hall field.

to about 100 v at an average n_e of the order of 10^{14} cm $^{-3}$, $T_e/T_0 > 2$, and $\omega_e \tau_e \approx 10$. It has been previously reported⁷ that in the shock tube the electrode conduction mechanism is the same as in the cold cathode arc. The minimum measured V_s of 20 v is in agreement with the combined anode and cathode sheath losses that have been obtained in such arcs.⁷ This voltage loss occurs in a region that is of the order of an ion mean free path from the electrode surface.

Two calculations were performed to determine the location of the additional electrode voltage loss. In one calculation, it was assumed that there were no thermal and velocity boundary layers and that the electrodes were perfect electron emitters. The theory of Argyropoulos⁵ was used to obtain the field, current, and plasma distribution for one of the xenon experiments at T_0 equal to 5670°K (see Table 1). An electrode current of 45 amp was specified, and B_z was 2.2 webers/m 2 . A constant-property solution and a finite-rate solution were obtained (Sec. III). The transverse variation of the plasma properties, obtained in the finite-rate solution, is shown in Fig. 8. The magnitude of n_e , σ_0 , and $\omega_e \tau_e$ in the core of the flow are identical in both the finite-rate and constant-property solutions. However, in the former case, Fig. 8 shows that a high-conductivity region extends from the electrode walls to a distance of about ρD (i.e., 4.8 mm). Figure 9 shows the variation of the transverse field in the plasma frame of reference, E_y^* , for the two solutions. It can be seen that the high-conductivity layers at the electrode walls greatly improve the uniformity of E_y^* . The results will be discussed further in Sec. V.2. For the purposes of the present discussion, the important result obtained from Figs. 8 and 9 is that the plasma non-uniformities extend a distance of about ρD (i.e., 4.8 mm) from the wall. In addition, the voltage loss due to the hot layers is only a few volts.

A second calculation was performed to determine the effect of the thermal boundary layer on the electrode voltage loss. The velocity boundary layer was neglected, and it was assumed that j_y and the plasma properties were constant in the axial x direction. Although j_y is not uniform near the electrode surface, the essential features of the solution can be exhibited more conveniently at constant j_y . At any point on the shock-tube wall, the boundary-layer thickness increases as $x^{1/2}$. To maximize the boundary-layer effect, the boundary-layer thickness at the end of the gas slug ($x \approx 50$ cm) was used. The computation was performed for one of the 98% neon + 2% xenon experiments at $T_0 = 2830^\circ\text{K}$ (see Table 1) and $j_y = 10$ amp/cm 2 . This case was chosen because the largest V_s values were obtained in this gas mixture. The shock-wave solution given by Duff¹⁵ was used to obtain the temperature profile in the boundary layer.

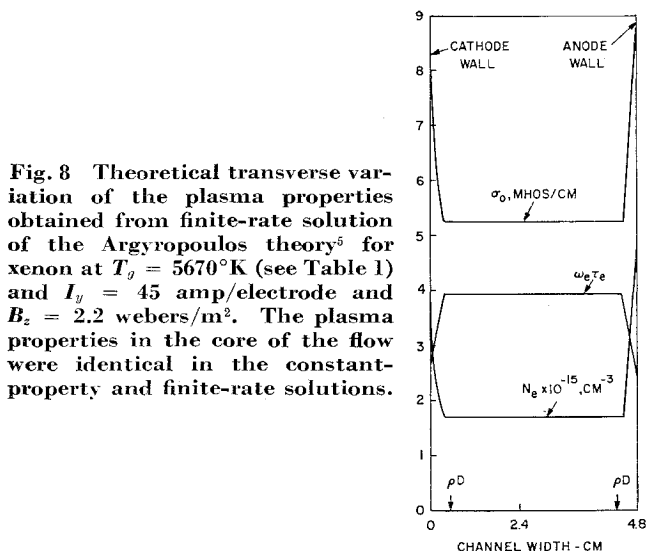


Fig. 8 Theoretical transverse variation of the plasma properties obtained from finite-rate solution of the Argyropoulos theory⁵ for xenon at $T_0 = 5670^\circ\text{K}$ (see Table 1) and $I_y = 45$ amp/electrode and $B_z = 2.2$ webers/m 2 . The plasma properties in the core of the flow were identical in the constant-property and finite-rate solutions.

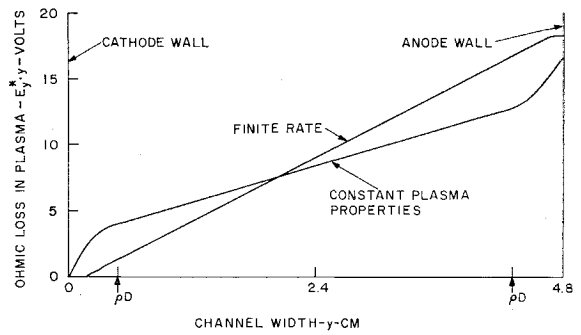


Fig. 9 Theoretical variation of the ohmic voltage loss in the plasma, E_y^* , as a function of the channel width. The pertinent plasma and generator conditions are the same as in Fig. 8. Both the constant-property and finite-rate solutions are shown.

The plasma properties obtained by using Eq. (3) with σ_0 are shown in Fig. 10 as a function of the distance from the electrode wall. E_y^* in Fig. 10 was obtained from j_y/σ_0 . The thermal boundary-layer thickness δ_T and the velocity boundary-layer thickness δ_U are indicated on the abscissa. The latter value is given by Mirels.¹⁶ It can be seen that almost the entire effect of the thermal boundary layer is concentrated within 1 mm from the electrode wall. In the 98% neon + 2% xenon experiment for which j_y was 10 amp/cm 2 , the measured value of V_s is about 80 v (Fig. 2). Subtracting 20 v for the previously mentioned sheath drops, the measured boundary voltage loss at each electrode is about 30 v. By substituting the results of Fig. 10 into Eq. (1), it was found that with the thermal boundary layer the voltage loss $E_y^* \cdot y$ is only 1 v greater than that obtained with the constant temperature solution. A 30-v boundary-layer loss can be obtained if it is arbitrarily assumed that $E_x = 0$ between $y = 0$ and $y = 1$ mm. However, the Argyropoulos solution for xenon, just cited, shows that $E_x \neq 0$ to within the order of mean free path from the electrode surface. Since the actual current conduction to the electrode occurs through localized "arc spots," the preceding simple analysis cannot be expected to describe the local behavior of the field near the electrode surface. However, two important conclusions can be drawn from this section. 1) From the Argyropoulos analysis one can conclude that high-conductivity layers near the electrode walls do not cause large electrode losses. 2) Regardless of the mechanism that causes the large electrode losses in the cold thermal boundary layer, these losses appear to occur in a region that is less than 1 mm from the wall. This thickness is less than 4% of the channel half-

Fig. 10 Theoretical variation of the field and plasma properties in the thermal boundary layer as a function of the distance from the electrode surface. The computations were performed for the 98% neon + 2% xenon mixture, at $T_0 = 2830^\circ\text{K}$ (see Table 1) and $j_y = 10$ amp/cm 2 , at a point that was 50 cm behind the shock front.

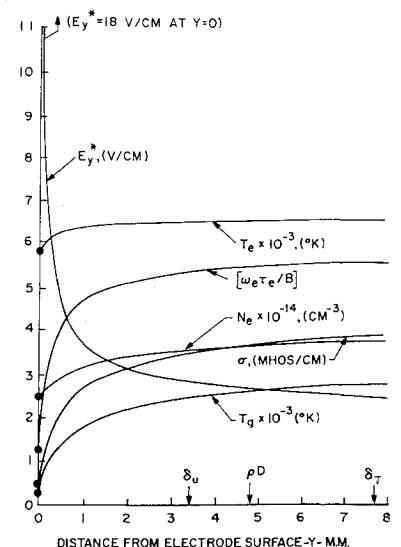


Table 2 Centerline values of E , J , and plasma properties obtained from ADK theory⁵ and experiment

Xenon	T_g , °K	B_z , weber/ m ²	T_e , °K	n_e , cm ⁻³	$\omega_e \tau_e$	I_y , amp	j_x , amp/ cm ²	j_y , amp/ cm ²	θ	E_x , v/cm	E_y^* , v/cm	$U_x B_z$, v/cm
1) Constant-property theory	5670	2.20	6390	1.68×10^{15}	3.94	45	0.28	-9.85	1.65°	-8.05	-2.30	-21.67
2) Finite-rate theory	5670	2.20	6394	1.7×10^{15}	3.93	45	2.40	-9.85	13.68°	-7.56	-4.02	-21.67
3) Experiment	5670	2.20	N.M. ^a	1.9×10^{15}	N.M.	45	N.M.	N.M.	N.M.	-6.25 ± 0.75	N.M.	-21.67
98% Neon + 2% Xenon												
4) Constant-property theory	2830	0.55	6652	3.66×10^{14}	3.46	45	0.28	-9.85	1.61°	-9.04	-2.98	-9.00
5) Finite-rate theory	2830	0.55	6726	3.98×10^{14}	3.38	45	0.46	-9.85	25.00°	-7.34	-6.62	-9.00
98% Neon + 2% Xenon												
6) Constant-property theory	2830	1.10	6654	3.66×10^{14}	6.80	45	0.30	-9.85	1.74°	-18.04	-3.31	-18.00
7) cycle 3	2830	1.10	6720	4.2×10^{14}	6.17	45	7.50	-9.85	37.00°	-15.70	-16.40	-18.00
8) Finite rate (unstable) cycle 7	2830	1.10	7110	7.7×10^{14}	5.00	45	17.70	-9.85	60.00°	-9.50	-27.30	-18.00
9) Shorted mode cycle 9	2830	1.10	7290	1×10^{15}	4.70	45	21.80	-9.85	66.00°	-11.70	-42.20	-18.00
10) Finite rate (unstable) cycle 8 Normal mode	2830	1.10	6680	4×10^{14}	6.75	45	3.04	-9.85	17.00°	-8.13	-4.48	-18.00
98% Neon + 2% Xenon												
11) Constant-property theory	2830	2.20	6650	3.67×10^{14}	12.74	45	0.47	-9.85	2.73°	-36.50	-4.26	-36.00
12) Experiment	2830	2.20	N.M.	1.3×10^{15}	N.M.	45	N.M.	N.M.	N.M.	-16.50	-11.00 (max.)	-36.00

^a No measurement.

height. Hence, one is justified in treating E_e as an equivalent external load.

2. Theory of Nonuniform Ionization in Segmented-Electrode Generator

In this section, the theory of Argyropoulos, Demetriades, and Kendig (ADK)⁵ will be compared to the experiments. Because of the complexity of the computational procedure, the ADK theory was applied to only two representative experimental conditions. The first was xenon at T_g of 5670°K (Table 1), where $(T_e/T_g) \approx 1$. The second was 98% neon + 2% xenon at T_g of 2830°K (Table 1), where (T_e/T_g) is relatively large. For comparison purposes, in all the computations I_y was fixed at 45 amp/electrode ($j_y = 10$ amp/cm²). Two parts of the solution will be presented. The plasma distribution in the channel will be given for comparison with the observed discharge structure. Also, the field, current, and plasma properties in the core of the flow will be given for comparison with the appropriate experimental results.

The distribution of the plasma properties obtained from the finite-rate solution for xenon at $I_y = 45$ amp/electrode and $B_z = 2.2$ webers/m² was presented in Sec. V.1 and Fig. 8. The variation of T_e , n_e , σ_0 , and $\omega_e \tau_e$ in the flow direction was negligibly small over the 0.96-cm-wide electrode pitch. In addition, the solution showed that within a distance of 5 mm from the electrode walls, n_e was considerably higher than in the core of the flow.[†] The foregoing theoretical results describe a steady-state case, and they are in disagreement with the experiments. Nonstationary, 1-cm-wide, transverse streamers were observed in the discharge.² Except for the entrance region, high-luminosity gas layers were not observed on the electrode walls at these current levels.² The discrepancy between theory and experiment results from neglecting in the theory the time dependence and the ionization relaxation process in the entrance region of the channel. The ADK theory uses the steady-state, nonequilibrium T_e as a boundary condition at the upstream side of the electrode segment.⁵ For the xenon computation, this value of T_e is 6390°K. At 6390°K, the characteristic length for changes in T_e in the flow direction

[†] It can be seen in Fig. 8 that n_e is higher at the anode than at the cathode. This behavior was observed in all the finite-rate solutions in which electron thermal diffusion was included in the computation. The higher n_e at the anode wall increases the Hall field shorting effect, and, hence, it can account for the observed asymmetry in E_x (see Sec. IV.4). However, in the theoretical calculations, no variation in E_x developed in the core of the flow.

is five times the 0.96-cm axial electrode pitch.¹⁷ However, it was shown¹ that in the entrance region of the channel an overshoot of T_e above its average steady-state value occurs. Thus, to provide a better description of the discharge structure in the present experiments, the entrance problem and the time dependence must be included in future analyses.

The results of the computations obtained in the core of the flow are summarized in Table 2. For convenience, the centerline values of the various parameters are shown. Appropriate experimental results are also shown in Table 2. The theoretical solution can be divided into two regimes with the dividing line occurring at $\omega_e \tau_e$ of about 4. Below this value of $\omega_e \tau_e$, the finite-rate solution converged for both the xenon and 98% neon + 2% xenon cases. The values of the parameters obtained with the constant-property and the finite-rate solutions in xenon at 2.2 webers/m² are tabulated in rows 1 and 2, of Table 1, respectively. The results show that the plasma nonuniformities increase the Hall current j_x from 0.28 amp/cm² in the constant-property case to 2.4 amp/cm². The large increase in j_x is caused by the high n_e layers on the electrode walls (see Fig. 8) which short the Hall field. As a result of the increase in j_x , the angle θ , where $\theta = \tan^{-1}(j_x/j_y)$, increases from 1.65° to 13.68° (see Table 1). Thus, transverse nonuniformities change the Faraday-generator operating mode from a normal (i.e., $\theta \approx 0^\circ$) to a shorted mode ($\theta \gg 0^\circ$). In the shorted mode, the dissipation in the plasma is higher, as evidenced by the increases in T_e and n_e in the finite-rate solution (Table 2, row 2). However, despite the large increase in j_x , E_x in the finite-rate solution is only 5% less than in the constant-property case. This result can be explained by noting that $\omega_e \tau_e$ decreases in the high-conductivity layers (see Fig. 8), thereby reducing the Hall field shorting effect at the wall. The decrease in $\omega_e \tau_e$ is caused by the increase in the coulomb collision frequency as n_e increases. A cold boundary layer can produce the same result⁴ in the absence of coulomb collisions. In contrast to the small reduction in E_x , E_y^* in the finite-rate solution is a factor of 2 larger than in the constant-property case. Thus, the xenon computations show, somewhat unexpectedly, that E_y^* is the critical measurable parameter that determines the mode of generator operation. Unfortunately, for the xenon case E_y^* is only 10 to 20% of $\mathbf{U} \times \mathbf{B}$ (see Table 2). In the present channel, such small values of E_y^* cannot be measured to sufficient accuracy to verify the theoretical calculation. (See discussion in Sec. III.2.) It can be seen that the experimental values of n_e and E_x (Table 2, row 3) are in approximate agreement with both theoretical computations. Hence, these measurements are inconclusive in verifying the finite-rate calcula-

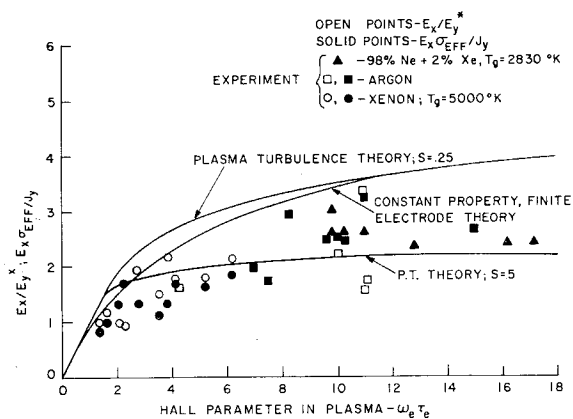


Fig. 11 Theoretical and experimental effective Hall parameter as a function of the local Hall parameter in the plasma. The plasma-turbulence theory of Louis⁶ and the finite-electrode theory of Hurwitz et al.³ were used to obtain the three theoretical curves.

tion. It is the absence of the high-luminosity gas layers on the electrode walls² which leads one to conclude that in xenon the generator operated in the normal mode. The theoretical results for the 98% neon + 2% xenon case at $B = 0.55$ webers/m² are tabulated in rows 4 and 5 of Table 2. Here $\omega_e \tau_e < 4$ and the solution converged. The solution has the same characteristics as in the xenon case. One can conclude that at low $\omega_e \tau_e$ convergence of the solution does not appear to be sensitive to the ratio of T_e/T_0 .

For $\omega_e \tau_e > 4$, the finite-rate solution did not converge in either the xenon case or in the 98% neon + 2% xenon case. It was not possible to perform a sufficient number of computations to determine the exact value of $\omega_e \tau_e$ at which the instability occurred. Using the criteria for the onset of the electrothermal instability, Argyropoulos¹⁸ determined that a value of $\omega_e \tau_e > 2.8$ was a necessary but not sufficient condition for the onset of instability. Since a converging steady-state xenon solution was obtained at $\omega_e \tau_e$ of 4, an additional mechanism is operative. The computations at $\omega_e \tau_e > 4$ commenced with θ generally increasing from cycle to cycle. After about the fifth cycle, θ suddenly decreased to a small angle which was either positive or negative. The solution then oscillated between cycles with large θ to cycles with small θ . In a considerably simplified version of this theory, Kerrebrock⁴ noted that at large $\omega_e \tau_e$ two solutions existed to the coupled electron conservation and the MHD-generator equations. One was the normal mode solution g , and the other was the shorted mode solution.⁴ It is tentatively suggested that the present analysis also attempts to generate these two solutions. A typical, unstable solution is shown for the 98% neon + 2% xenon mixture at $B_z = 1.1$ webers/m² in Table 2, rows 6-10. Row 6 gives the constant-property solution. The next three rows show cycles 3, 7, and 9 of the shorted-mode, finite-rate solution. One notes that the dissipation in the plasma increases with increasing θ . Despite the large values of j_x , E_x in cycle 9 is only a factor of 2 lower than in the constant-property case. On the other hand, the corresponding increase in E_y^* is over a factor of 10. This behavior is similar to that in xenon at low $\omega_e \tau_e$ (Table 2, row 2). Considerable uncertainty about the actual value of θ exists in the normal mode solution, of which one example is shown in Table 2 (cycle 8). One notes that in this case the dissipation is smaller and that E_y^* is considerably smaller than in the shorted mode. It is interesting to note that E_x is about the same in the shorted and normal mode solutions. The 98% neon + 2% xenon experiments were performed at B_z of 2.2 webers/m². Although a theoretical computation was performed for this case, a value of ρ of 0.2 (in the present channel, $\rho = 0.1$) was used in the computation. The solution was similar to

the $B_z = 1.1$ -webers/m² case and it will not be given. The experimental results for the 2.2-webers/m² case are given in Table 2, row 12. The experimental E_x is a factor of 2 less than the "constant" property value. By comparison with the relative values of E_x in the $B_z = 1.1$ -webers/m² theoretical solution, it is clear that in this case E_x cannot be used to determine the generator mode of operation. Because of the large scatter in the probe data in Fig. 2, the value of E_y^* of 11 v/cm (Table 2, row 12) was obtained by noting that all the probe measurements on the average gave a value of about 120 v. The theory in Fig. 2 shows that E_y^* is nearly independent of I_y . Hence, by neglecting the $\mathbf{J} \times \mathbf{B}$ effect, one obtains a maximum E_y^* of $(175-120 \text{ v})/4.85 \text{ cm} \cong 11 \text{ v/cm}$. With the Lorentz force effect included, it is estimated that E_y^* is about half of this value. Comparing the experimental E_y^* with the theoretical values obtained in the shorted mode solution at 1.1 webers/m², one can conclude that the generator operated in the normal mode.

3. Effect of Electrothermal Instability on the Generator Performance

The electrothermal instability theory predicts the onset of plasma nonuniformities and fluctuations at $\omega_e \tau_e > 1$. The nonuniformities decrease σ_{eff} and $(\omega_e \tau_e)$, whose magnitudes depend on the assumptions made^{6,11-14} regarding the structure of the plasma nonuniformities. The theories^{6,11-14} neglect the effect of finite electrodes in the linear Faraday generator on the magnitudes of σ_{eff} and $(\omega_e \tau_e)_{eff}$. In addition, the direction of \mathbf{J} , which must be known to compute $(\omega_e \tau_e)_{eff}$ cannot be measured directly in a linear Faraday generator. To compare the experiments to the predictions of the instability theory, it was assumed that \mathbf{J} was parallel to $\mathbf{U} \times \mathbf{B}$ (or, equivalently, E_y). The validity of this assumption is based on the discussion in Sec. V.2, where it was shown that the present generator operates in the normal mode. With this assumption, $(\omega_e \tau_e)_{eff} \equiv (E_x/E_y^*) \equiv (E_x \sigma_{eff}^* / J_y)$. Figure 11 summarizes the results of the computations of the theoretical and experimental $(\omega_e \tau_e)_{eff}$ as a function of the local $\omega_e \tau_e$ in the plasma. For a uniform plasma, $(\omega_e \tau_e)_{eff}$ is given by Eq. (2). The result is given by the curve labeled "constant property, finite electrode theory" in Fig. 11. To compute the effect of electrothermal instabilities on $(\omega_e \tau_e)_{eff}$, the formulation given by Louis⁶ was selected. Assuming that the plasma is homogeneously turbulent, Louis derives an expression for $(\omega_e \tau_e)_{eff}$ as a function of $\omega_e \tau_e$ and S . Although in the present experiments the plasma is not homogeneously turbulent,² Louis' formulation was chosen because S can be measured from the fluctuations in the continuum radiation of the plasma. In the present experiments, the measured value² of S ranged from 0.25 to 0.5. For these two values of S , one obtains the two theoretical curves labeled "plasma-turbulence theory" in Fig. 11. In the experimental data reduction for Fig. 11, the plasma properties required to compute $\omega_e \tau_e$ and σ_{eff} were obtained from Eq. (3) with σ_{eff} substituted for σ . The experimental data in Fig. 11 were derived from the Hall data in Figs. 3, 4, and 6. The open points in Fig. 11 represent the ratio E_x/E_y^* . Since E_y^* is subject to relatively large errors (see Sec. IV.2), the E_x/E_y^* data have a great deal of scatter. Accordingly, the experimental $(\omega_e \tau_e)_{eff}$ was also computed from $(E_x \sigma_{eff}^* / J_y)$. These latter data points are not completely experimental in that σ_{eff} is defined theoretically. It can be seen in Fig. 11, that for $\omega_e \tau_e > 4$, the experimental $(\omega_e \tau_e)_{eff}$ scatters between 1.5 and 3.3. For $\omega_e \tau_e > 4$, the data lie between the two theoretical curves obtained from the plasma-turbulence theory, and it is within a factor of 2 of the constant-property theory. The other theoretical derivations¹²⁻¹⁴ of the effect of instabilities on $(\omega_e \tau_e)_{eff}$ generally predict that, at large $\omega_e \tau_e$, $(\omega_e \tau_e)_{eff}$ saturates at values between 1 and 2. Saturation of $(\omega_e \tau_e)_{eff}$ at values below 2 has been widely observed (e.g., Refs. 4 and

6) in experiments in various MHD channel configurations. Although some of the data in Fig. 11 lies at values of $(\omega_e \tau_e)_{eff}$ greater than 2, the scatter in the data is too large to establish conclusively whether the Faraday-generator performance is limited by the finite-electrode effect or by the electrothermal instabilities. To resolve this question, experiments with finer electrode regimentation ratios will be necessary. However, it should be noted that a number of predictions of the electrothermal instability theory disagree with experimental observations in the present MHD channels. The details are given elsewhere.² Finally, the experimental data in Fig. 11 also show that the generator operated in the normal mode, since in the shorted mode the ratio of (E_x/E_y^*) is much less than one. (See Table 2.)

VI. Summary and Conclusions

The major result of this study was that the nonequilibrium Faraday generator operated in the normal mode, in the range of $\omega_e \tau_e$ of 1 to 20 used in the experiments. To the authors' knowledge this is the first nonequilibrium generator in which normal-mode operation persisted to high values of $\omega_e \tau_e$. The conclusion concerning normal mode operation is primarily based on the following two results obtained from the ADK theory⁵: 1) The experimentally determined transverse fields E_y^* were consistent with the theoretically predicted values for normal mode operation, and they were much smaller than the theoretical values corresponding to the shorted mode of generator operation. 2) High-conductivity layers on the electrode walls, which according to the theory must exist for shorted mode operation, were not observed in the experiments.

The following additional results were obtained from the application of the ADK theory to the experimental conditions: 1) At $\omega_e \tau_e > 4$, the theoretical solution failed to converge, and it oscillated between the normal and shorted mode cases. 2) The failure of the theory to predict the experimentally observed discharge structure was attributed to the neglect of the time dependence and the generator entrance effects in the analyses. 3) E_y^* was a very sensitive indicator of the generator mode of operation. On the other hand, the average Hall field was a relatively insensitive indicator of the mode of generator operation.

It was shown that the accuracy of the electric field measurements depends upon the impedance of the probe measuring circuit. With a sufficiently high probe impedance, the accuracy of the E_y^* measurements was still reduced by the presence of large electrode voltage losses, plasma non-uniformities, and the reduction in the gas velocity by the Lorentz force. On the other hand, the Hall field measurements were generally unaffected by these three effects.

It was found that a simple theory based on the constant-property, finitely segmented electrode theory³ could be used to reduce the data. The transverse voltage-current characteristics were in reasonably good agreement with this theory if the following factors were included in the analysis: 1) The reduction of the gas velocity by the Lorentz force. 2) The use of the effective tensor conductivity, instead of the scalar conductivity, in the electron energy equation; this modification was required to account for the increased ohmic dissipation resulting from the streamer discharge structure. 3) The treatment of the measured electrode voltage loss as an equivalent external impedance; this was justified in a series of computations which showed that the electrode losses occur in a region that is less than 4% of the channel half-height. The measured Hall fields were always within a factor of 2 of the values predicted by the simple theory.³ For $T_e/T_g > 1$, the discrepancy in E_x was because of the

underestimation of the actual electron density in the generator by the modified electron energy equation. For $(T_e/T_g) \approx 1$, the discrepancy in E_x was because of the neglect in the analyses of the gas heating caused by the Lorentz force. Finally, the observed transverse variation in E_x was attributed to local shorting of the discharge at the anode wall only by the Lorentz force.

A comparison of the experiments with the electrothermal instability theories showed that it was not possible to separate conclusively the effect of the relatively coarse electrode segments from the effect of the instability on the magnitude of the average Hall parameter. It is concluded from this study that a larger MHD channel is required to reduce the effect of electrode losses and coarse electrode segmentation ratios on the generator performance.

References

- Zauderer, B., "Experimental Study of Nonequilibrium Ionization in a Linear MHD Generator," *AIAA Journal*, Vol. 6, No. 4, April 1968, pp. 701-707.
- Zauderer, B., "Discharge Structure and Stability in a Linear, Non-Equilibrium MHD Channel," Paper 67-718, 1967, AIAA.
- Hurwitz, H., Jr., Kilb, R. W., and Sutton, G. W., "Influence of Tensor Conductivity on Current Distribution in an MHD Generator," *Journal of Applied Physics*, Vol. 32, 1961, pp. 205-216.
- Kerrebrock, J. L., "Segmented Electrode Losses in MHD Generators with Nonequilibrium Ionization," *AIAA Journal*, Vol. 4, No. 11, Nov. 1966, pp. 1938-1947.
- Argyropoulos, G. S., Demetriades, S. T., and Kendig, A. P., "Current Distribution in Non-Equilibrium $J \times B$ Devices," *Journal of Applied Physics*, Vol. 38, 1967, pp. 5233-5239.
- Louis, J. F., "Effective Ohm's Law in a Partially Ionized Gas with Electron Density Fluctuations," *The Physics of Fluids*, Vol. 10, 1967, pp. 2062-2064.
- Zauderer, B., "Electrical Characteristics of Linear Hall and Faraday Generators at Small Hall Parameters," *AIAA Journal*, Vol. 5, No. 3, March 1967, pp. 575-581.
- Zauderer, B., "Electrical Characteristics and Loss Mechanisms of a Non-Equilibrium Linear MHD Generator," *Proceedings of the Third International Symposium on MHD Electrical Power Generation*, OECD/ENEA, Vol. II, 1966, pp. 450, 597-611.
- Sherman, A., "MHD Channel Flow with Non-Equilibrium Ionization," *The Physics of Fluids*, Vol. 9, 1966, pp. 1782-1787.
- Oliver, D. A. and Mitchner, M., "Nonuniform Electrical Conduction in MHD Channels," *AIAA Journal*, Vol. 5, No. 8, Aug. 1967, pp. 1424-1432.
- Kerrebrock, J. L., "Non-Equilibrium Ionization Due to Electron Heating, Part I, Theory," *AIAA Journal*, Vol. 2, No. 6, June 1964, pp. 1072-1080.
- Velikhov, E. P. and Dykhne, A. M., "Plasma Turbulence Due to Ionization Instability in a Strong Magnetic Field," *Proceedings of the Sixth International Symposium on Ionization Phenomena in Gases*, European Nuclear Energy Agency, Vol. IV, 1963, pp. 511-512.
- Solbes, A., "Nonlinear Plane Wave Study of Electrothermal Instability in Non-Equilibrium Plasmas," *Proceedings of the Eighth Symposium on the Engineering Aspects of MHD*, Stanford Univ., 1967, pp. 110-112.
- Vedenov, A. A. and Dykhne, A. M., "Effective Conductivity of Plasma in a Magnetic Field," *Proceedings of the Third International Symposium on MHD Electrical Power Generation*, OECD/ENEA, Vol. II, 1966, pp. 335-343.
- Duff, R. E., "Laminar Boundary Layer Development Behind Shock Waves in Argon," *The Physics of Fluids*, Vol. 1, 1958, pp. 546-547.
- Mirels, H., "Correlation Formulas for Laminar Shock Tube Boundary Layers," *The Physics of Fluids*, Vol. 9, 1966, 1265-1272.
- Lackner, K., Argyropoulos, G. S., and Demetriades, S. T., "Relaxation Effects in $J \times B$ Devices," *AIAA Journal*, Vol. 6, No. 5, May 1968, pp. 949-951.
- Argyropoulos, G. S., private communications.